Current Chemistry Letters 2 (2013) 77–84

Contents lists available at Growing Science

Current Chemistry Letters

homepage: www.GrowingScience.com/ccl

The removal of 2,4-dichlorophenol under visible light irradiation by silver indium sulfide nanoparticles synthesized by microwave

Azadeh Tadjarodi*, Amir Hossein Cheshme khavar and Mina Imani

Research Laboratory of Inorganic Materials Synthesis, Department of Chemistry, Iran University of Science and Technology, Narmak, Tehran, 16846-13114, Iran

CHRONICLE

Article history:
Received October 28, 2012
Received in Revised form
December 6, 2012
Accepted 27 February 2013
Available online
1 March 2013

Keywords:
AgInS2
Nanoparticles
Photodegradation
Dichlorophenol
Microwave

ABSTRACT

Silver indium sulfide ($AgInS_2$) nanoparticles were synthesized by microwave method. These nanopartricles were characterized by FT-IR, XRD, DRS, SEM and TEM techniques. The band gap energy of 1.96 eV was determined by UV-Vis diffuse reflection spectrum (DRS). The photocatalytic activity was studied by photodegradation reaction of 2,4-dichlorophenol (2,4-DCP) under visible light irradiation. The influence of initial concentration, initial solution pH on the degradation percentage of 2,4-DCP and also, the kinetics of photodegradation were investigated. The removal efficiency up to 95% proved the superior capability of $AgInS_2$ (AIS) nanoparticles for water purification.

1. Introduction

The chlorophenols are extensively used as fungicide, herbicide, wood preservative, dyes and drugs[1-2]. These materials have been listed as toxic pollutants by the various environmental protection agencies such as the United States Environmental Protection Agency[3]. The increase of discharging these materials from the industrial and domestic activities into the environment leads to enhance the waters pollution. Being toxic and harmful for environment and living organisms and the shortage of water sources, these pollutants should be removed. Nowadays, the variety of photocatalysts is employed for solving the serious environmental and pollution challenges[3-5]. In fact, the use of photocatalysis technology for destruction of the organic pollutants in water is an interesting method,

* Corresponding author. Tel: +98 21 77240359
E-mail addresses: tajarodi@iust.ac.ir (A. Tadjarodi)

doi: 10.5267/j.ccl.2013.03.001

which can be replaced to the traditional methods[6-10]. In this technique, the active species such as $OH^{\bullet}$, $O_2^{\bullet-}$ and hole (h^+) are generated by light energy and performed the degradation of organic pollutants[10-11]. Although, the semiconductors such as TiO_2 and ZnO with a wide band gap of 3.23-3.37 eV are the best operational available, these are only activated under UV light irradiation, which accounts for around 5% of the total solar energy. Therefore, a decreased band gap can extend the photocatalytic application from UV light region into the visible light range[12-13].

Many studies have been carried out to exploit the new semiconductor materials with a narrow band gap adapted to the visible light domain. $AgInS_2$ is a ternary chalchogenide with direct band gap about 1.86-2.03 eV and high extinction coefficient in visible light region[14-19]. Thus, this compound can be introduced as a favorable material for photovoltaic and photocatalytic applications. There are several routes for preparation of $AgInS_2$ nanoparticles[10, 14-16, 18, 20-26]. One of these methods is microwave irradiation process.

In the present study, $AgInS_2$ nanoparticles with the pure orthorhombic phase were synthesized by the microwave method. The photocatalytic activity of $AgInS_2$ nanoparticles was investigated for degradation of 2,4-dichlorophenol (2,4-DCP) under visible light irradiation.

2. Results and Discussion

2.1. Structural and morphological study

Fig. 1 shows the XRD pattern of the synthesized AIS sample. All of the diffraction peaks confirm the crystalline phase of orthorhombic $AgInS_2$ (JCPDS No. 25-1328). In addition, no characteristic peaks of the impurities are observed in this pattern, implying that a pure orthorhombic phase of $AgInS_2$ has been synthesized.

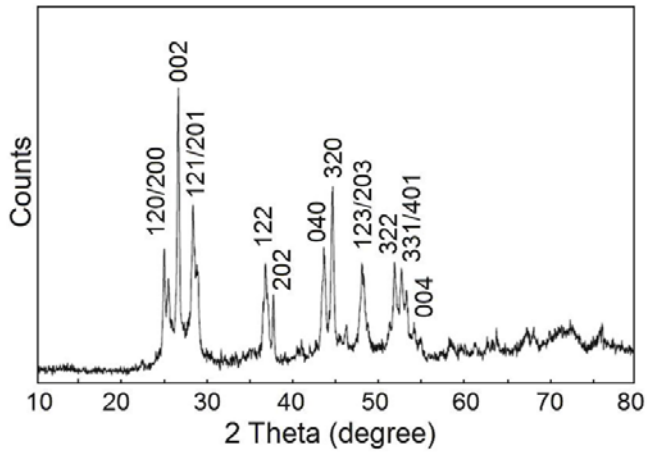

Fig. 1. XRD pattern of $AgInS_2$ nanoparticles

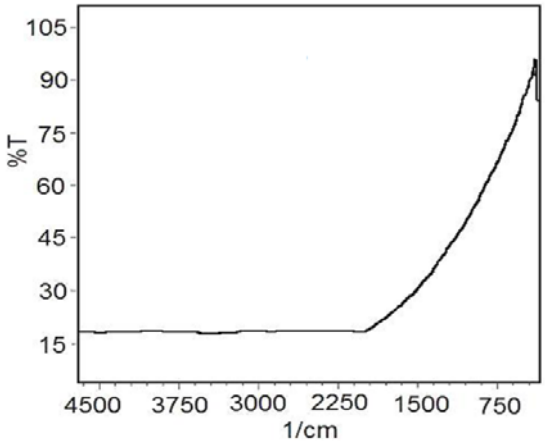

Fig. 2. FT-IR spectrum of $AgInS_2$ nanoparticles

FT-IR spectrum shown in Fig. 2 confirmed the purity of the obtained product. There are no peaks in this spectrum, which represents the removal of organic sections *via* washing with ethanol and distilled water. The morphology of as-synthesized product was studied by SEM and TEM techniques. The SEM images revealed the uniform particulate morphology with the average particle size of 70 nm (Figs. 3a and b).

The TEM image shown in Fig. 3c further confirmed the results of SEM technique. The average particle size was estimated using a microstructure measurement program and Minitab statistical software[27, 28]. The histogram of the particles size distribution of the obtained sample has been illustrated in Fig. 3d.

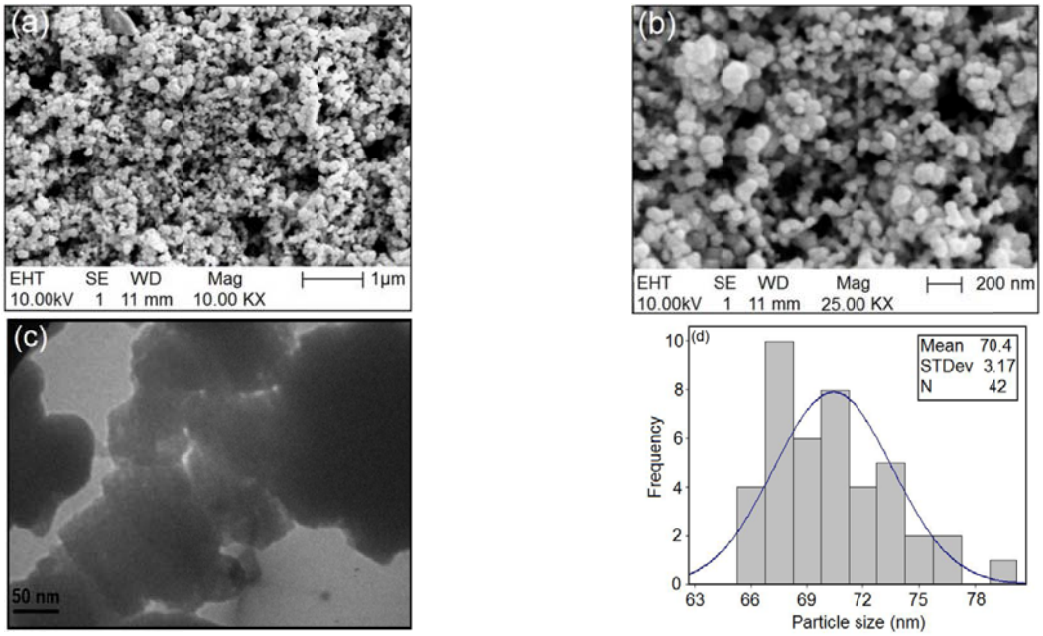

Fig. 3. SEM images (a-b), TEM image (c) and the statistical graph of particle size distribution (d) of $AgInS_2$ nanoparticles

The nitrogen adsorption and desorption experiments were performed for determining the surface area of these nanoparticles. A distinct hysteresis loop recorded at the range of $0<P/P_0<1$ indicated the category of type V (Fig. 4). The Brunauer-Emmett-Teller (BET) surface area about 5.9 m^2g^{-1} was calculated for synthesized product. The Barrett-Joyner-Halenda (BJH) model using desorption branch of the nitrogen isotherm was applied to evaluate the pore size distribution of AIS nanoparticles, which was centered at 1.64 nm (inserted in the inset of Fig. 4). It is an acceptable value for AIS nanoparticles in comparison with the other reports[10], which can be referred to the presence of active sites on the surface of AIS nanoparticles.

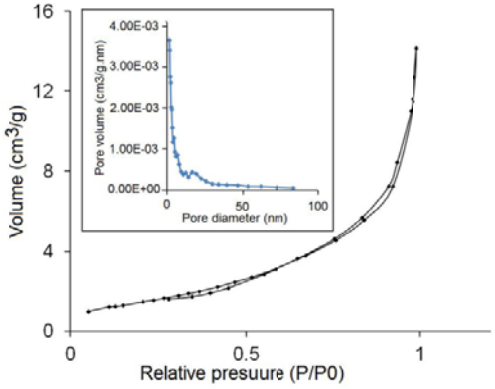

Fig. 4. Nitrogen adsorption (♦) and desorption (▲) isotherms for the AIS nanoparticles. The inset shows BJH plot of this product

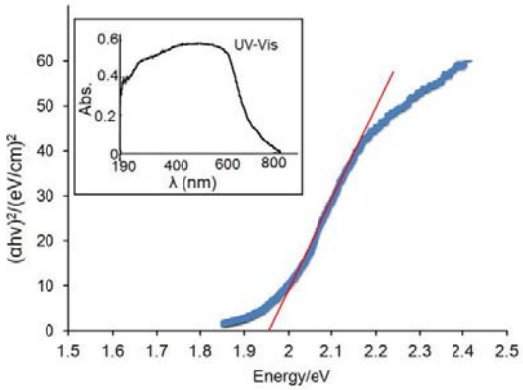

Fig. 5. The plot of $(\alpha h\nu)^2$ *vs.* hν (eV) for determining the direct band gap energy of the prepared $AgInS_2$ nanoparticles with UV-Vis spectrum in the inset

2.2. The optical property

The optical property of the AIS nanoparticles was investigated by the band gap energy determination using UV–Vis DRS. In order to calculate the direct band gap of the prepared sample was used Tauc relation[24]:

$$(\alpha h\nu)^2 = B(h\nu - E_g) \quad (1)$$

Where, α is the absorption coefficient, hν is the photon energy, B is a constant value and Eg is the band gap energy. In equation (1), the absorption coefficient (α) is estimated by the following equation:

$$\alpha = \frac{-1}{t} \ln T, \tag{2}$$

where, T is the transmittance value and t is the thickness of the substance that is exposed to the UV-Vis irradiation. Based on the UV-Vis DRS, the plot of $(\alpha h\nu)^n$ *vs*. hν in eV was drawn. The band gap value was obtained by extrapolating the linear region of this curve. Fig. 5 shows the band gap energy plot with the UV-Vis absorption spectrum in the inset. The measured band gap was found to be 1.96 eV. This value indicates that this nanomaterial can be liable for the phtocatalytic activity in visible light domain.

2.3. Photodegradation performance of AIS nanoparticles

In order to study the phtodegradation performance of AIS nanoparticles, a series of the comparative experiments were carried out in purification of polluted water with 2,4-DCP under visible light irradiation. After 6 h of light irradiation time, the remained concentration of pollutant in aqueous solution was determined.

The removal efficiency of phtocatalytic activation was concluded from Eq. 3:

$$\text{Removal efficiency} = \frac{C_0 - C_t}{C_0} \times 100\% \tag{3}$$

where, C_0 is the initial 2,4-DCP concentration and C_t is the pollutant concentration at time, t. All C_0 and C_t values were determined by the maximum absorption at the wavelength of 248 nm. The progress of the photocatalytic degradation of 2,4-DCP under visible light illumination was monitored by UV-Vis spectrophotometer. It was found that no degradation of 2,4-DCP was occurred in the absence of the photocatalyst under visible light irradiation. When the photocatalytic reaction was carried out in the dark, the removal efficiency of 3% is resulted. In fact, it is originated from the partial adsorption of the organic molecules on the surface of photocatalyst particles. Degradation performance was significantly improved up to 95%, when the 2,4-DCP solution containing AIS nanoparticles was exposed to the visible light illumination (Fig. 6).

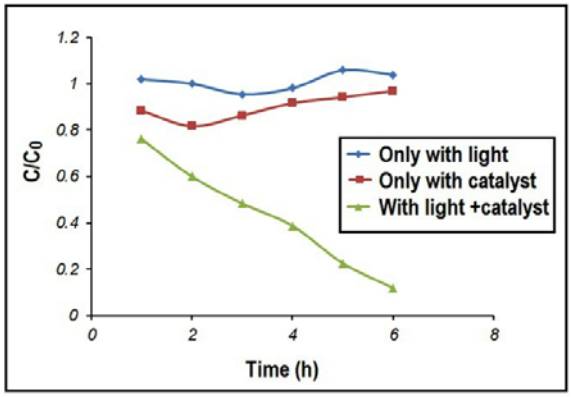

Fig. 6. Dependence of degradation of 2,4-DCP to the presence of light and catalyst

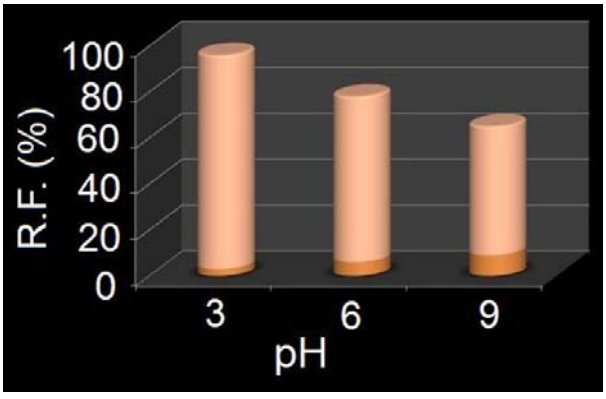

Fig. 7. The effect of initial solution pH on the degradation percentage of 2,4-DCP

2.3.1. Initial solution pH

The effect of solution pH on the degradation of 2,4-DCP was investigated *via* adjusting solution pH to three values of 3, 6 and 10 by 0.01 mol L^{-1} HCl and NaOH, respectively. Each of these runs was performed in the aqueous solutions of 2,4-DCP with 15 mg L^{-1} concentration (50 mL) containing 0.02 g AIS photocatalyst. Fig. 7 shows the degradation operation at different pH values. An enhanced removal percentage (95%) was observed at pH=3. This value declines to 81 and 43% at adjusted solution pH to 6 and 10, respectively. According to the mentioned results, the initial solution pH of 3 was selected for further studies.

2.3.2. Initial 2,4-DCP concentration

In order to study the influence of initial 2,4-DCP concentration on the removal efficiency, three initial pollutant concentrations *i.e.*, 15, 25 and 50 mg L^{-1} were examined. The results have been exhibited in Fig. 8. Due to increase the 2,4-DCP concentration from 15 to 25 and 50 mg L^{-1}, the removal percentage of 2,4-DCP decreased from 95 to 80 and 70%, respectively. This result can be ascribed to reduce the active sites on the catalyst surface. Meanwhile, the increase of pollutant concentration can decrease the light transmittance within suspension. Both of these reasons lead to decline the amount of hydroxyl radicals ($OH^{\bullet}$) in medium and subsequently, the reduction of removal efficiency.

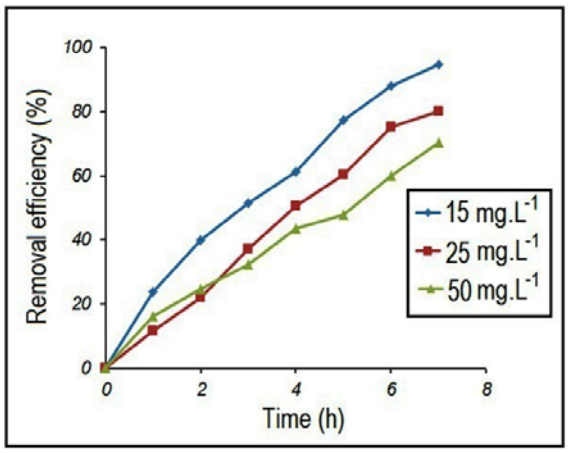

Fig. 8. Dependence of the removal efficiency to initial 2,4-DCP concentration in various irradiation times

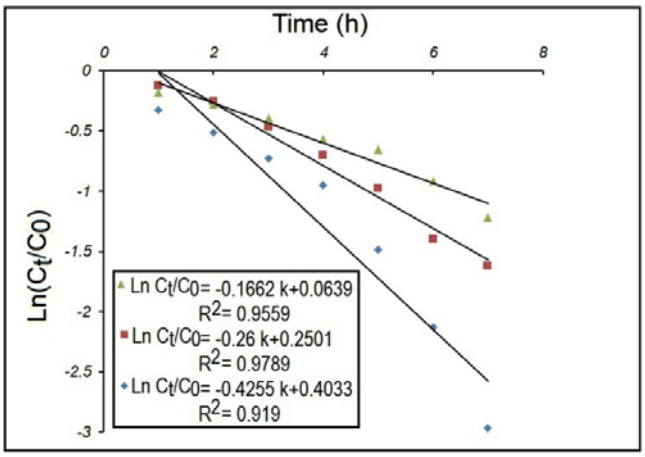

Fig. 9. The kinetics model of photodegradation performance of the $AgInS_2$ nanoparticles, initial 2,4-DCP concentration of 15, 25 and 50 mg L^{-1}, initial solution pH of 3 with the charge of fixed amount of photocatalyst (0.02 g)

2.3.3. Kinetic evaluation

The scanning of photocatalytic reaction indicated that this operation can be described by the simplified kinetic model of pseudo first-order equation and its formula is given as:

$$Ln\ (\frac{Ct}{C_0}) = -kt \quad (4)$$

where, C_0 is the initial concentration (mg L^{-1}) and C_t is the concentration at time, t, the slope, k, is the apparent rate constant. By plotting Ln (C_t/C_0) vs. time, a linear relationship was observed for each of three experiments with different concentrations (Fig. 9). The results represented that the photocatalytic activity of AIS nanoparticles for removing the 2,4-DCP from aqueous solution follows the pseudo-first-order kinetic model. As seen in Fig. 9, the correlation coefficients (R^2) of pseudo-first-order model are 0.955, 0.978 and 0.919 for applied 2,4-DCP concentrations (15, 25 and 50 mg L^{-1}), respectively. The all of three experiments show good fit to pseudo-first-order model, but the

photocatalytic experiment with the 2,4-DCP concentration of 25 mg L^{-1} has a better fit than the other initial 2,4-DCP concentrations applied in this work.

2.3.4. Photodegradation mechanism

Generally, in a photocatalytic process, the excitation of electrons from valence band (VB) to conduction band (CB) and generation of electron–hole pairs take place on the surface of the photocatalyst by exposing to light irradiation. The exited electrons in CB and hole (h^+) in VB are captured by oxygen molecules and OH^- or H_2O species dissolved in the suspension, respectively. The transfer of electron to oxygen molecule generates the superoxide anion and also, the presence of h^+ on VB band leads to produce hydroxyl radical ($OH^•$). These species depredate the organic pollutant adsorbed by the catalyst surface. The attack of produced radicals to aromatic carbon with its unpaired electron of 2,4-DCP molecule leads to break the π-bond of the aromatic ring, dechlorination and the C-O bond formation. As a result, some by-products such as hydroquinone and quinoid structures maybe produced. Finally, degradation of 2,4-DCP is completed through forming of CO_2, H_2O and Cl^- as the final products [1-3], as shown in Scheme 1.

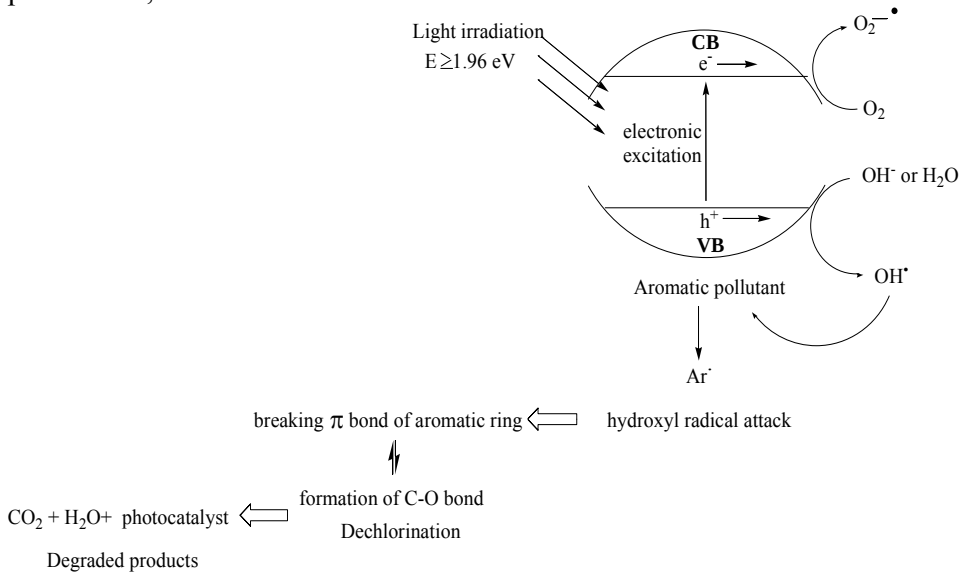

Scheme 1. The probable mechanism of phtocatalytic degradation of 2,4-DCP on the surface of $AgInS_2$ nanoparticles under visible light irradiation

3. Conclusions

In summary, $AgInS_2$ nanoparticles were successfully prepared by a rapid and facile microwave heating technique using $AgNO_3$, $InCl_3.4H_2O$ and thioacetamide as the starting materials. The structural and morphological studies confirmed the formation of a pure orthorhombic phase of $AgInS_2$ nanoparticles with the average size of 70 nm. The conformity of the band gap energy of this product (1.96 eV) with the visible region of solar energy suggested that the obtained nanoparticles can be employed as an appropriate phtocatalyst in this domain. A series of phtocatalytic reactions for degradation of 2,4-DCP as a pollutant model under visible light illumination were carried out. Meanwhile, a comparative study of the effective parameters on the photocatalytic performance was studied. As a result, the degradation process of 2,4-DCP was dependent on pH, and maximum removal efficiency (95%) was obtained at pH of 3. It was found that the phtodegradation of 2,4-DCP on the AIS nanoparticles at different concentrations follows a kinetics model of pseudo-first-order rate. The results suggested the high capability of AIS nanoparticles for water and wastewater treatment under visible light irradiation.

Acknowledgements

The financial support of this study, by Iran University of Science and Technology and Iranian Nanotechnology Initiative, is gratefully acknowledged.

Experimental

Materials

All reagents like indium (III) chloride tetrahydrate ($InCl_3.4H_2O$), silver nitrate ($AgNO_3$), ethylene glycol, sodium dodecyl sulfate (SDS) and thioacetamide (C_2H_5NS) were purchased from Merck Co. and used without further purification.

Characterization

The X-ray diffraction (XRD) pattern was recorded by a JEOL diffractometer using Cu Kα radiation (wavelength = 1.5418 Å). Scanning electron microscopy (SEM) images were taken on a Philips XL-30E SEM with gold coating. Transmission electron microscopy (TEM) images were measured on a ZEISS EM900 microscope working at 50 kV. Fourier transform infrared (FT-IR) spectrum was recorded on a Shimadzu-8400S spectrometer in the range of 400-4000 cm^{-1} using KBr pellets. The surface area of the product was obtained by using Brunauer-Emmett-Teller (BET) technique with Micromeritics (Gemini) in the range of relative pressures from 0.0 to 1.0. Before employing, the sample was degassed at 200 ºC for 2 h. In addition, the pore size distribution was determined from the desorption branch of the isotherm curve using the Barrett-Joyner-Halenda (BJH) model. The diffuse reflectance spectroscopy (DRS) was obtained using Shimadzu-UV-2550-8030 spectrophotometer in the range of 190-800 nm with slit width of 5.0 nm and light source with wavelength of 360.0 nm at room temperature.

General procedure

$AgInS_2$ nanoparticles were prepared by microwave method[20]. In a summary, 58 mg silver nitrate ($AgNO_3$), 100 mg indium (III) chloride tetrahydrate ($InCl_3.4H_2O$) and 51 mg thioacetamide (C_2H_5NS) were dissolved in ethylene glycol, separately. After mixing the solutions, sodium dodecyl sulfate (SDS) as a surfactant was added to this solution. The resulting mixture was stirred and placed into a domestic microwave oven with the power of 900 W for 5 min. The obtained precipitation was filtered and dried at 70 ˚C for 4 h in a vacuum oven.

Photocatalytic activity measurements

In this study, the photocatalytic behavior of the prepared AIS nanoparticles was evaluated *via* a probe reaction on the degradation of 2,4-dichlorophenol (2,4-DCP) in aqueous medium under visible light irradiation. A series of experiments were conducted to evaluate the influence of initial solution pH (with pH values of 3, 6 and 10) and initial 2,4-DCP concentration (15, 25 and 50 mg L^{-1}) on the photodegradation percentage. The fixed amount of photocatalyst (0.02 g) was charged into the reaction vessels. The solution was stirred for 1 h under dark conditions to establish the adsorption-desorption equilibrium. At given intervals of irradiation (60 min), 3 mL of suspension was taken away from the reaction vessels, centrifuged for 20 min to remove the remained catalyst from the solution. The visible light irradiation was carried out by a High-pressure mercury-vapor lamp (500W and λ=546.8 nm). The progress of photocatalytic reactions was monitored using the UV-Vis spectrophotometer at the wavelength of 315 nm.

References

1. Choi J. W., Chung S. G., Cho K. Y., Baek K. Y., Hong S. W., Kim D. J., Lee S. H. (2012) Photocatalytic Degradation of Chlorophenol Compounds using Poly Aromatic Star Copolymer. *Water Air Soil Pollut.*, 223, 1437-1441.

2. Jia J., Zhang S., Wang P., Wang H. (2012) Degradation of high concentration 2,4-dichlorophenol by simultaneous photocatalytic–enzymatic process using TiO_2/UV and laccase. *J. Hazard. Mater*., 205-206, 150-155.
3. Liu L., Chen F., Yang F., Chen Y., Crittenden J. (2012) Photocatalytic degradation of 2,4-dichlorophenol using nanoscale Fe/TiO_2. *Chem. Eng. J.,* 181– 182, 189-195.
4. Bayarri B., González O., Maldonado M. I., Giménez J., Esplugas S. (2007) Comparative Study of 2,4-Dichlorophenol Degradation With Different Advanced Oxidation Processes. *Trans. ASME.,* 129, 60-67.
5. Zhenxiang G. Li, C., Cheng S., Wei B., Xin Y. (2010) Photocatalytic degradation of 2,4- dichlorophenol using granular activated carbon supported TiO_2. *Desalination,* 263, 107-112.
6. Mele G., Del Sole R., Vasapollo G., García-López E. (2003) Photocatalytic degradation of 4-nitrophenol in aqueous suspension by using polycrystalline TiO_2 impregnated with functionalized Cu(II)–porphyrin or Cu(II)–phthalocyanine. *J. Catal.,* 217, 334-342.
7. Mele G., Ciccarella G., Vasapollo G., Garcia-López E. (2002) Photocatalytic degradation of 4-nitrophenol in aqueous suspension by using polycrystalline TiO_2 samples impregnated with Cu(II)-phthalocyanine. *App. Catal. B: Environ.,* 38, 309-319.
8. Wang C., Li J., Mele G., Yang G. M., Zhang F. X., Palmisano L., Vasapollo G. (2007) Efficient degradation of 4-nitrophenol by using functionalized porphyrin-TiO_2 photocatalysts under visible irradiation. *Appl. Catal. B: Environ*., 76, 218-226.
9. Marais E., Klein R., Antunes E., Nyokong T. (2007) Photocatalysis of 4-nitrophenol using zinc phthalocyanine complexes. *J. Mol. Catal. A: Chem.,* 261, 36-42.
10. Zhang W., Li D., Chen Z., Sun M., Li W., Lin Q., Fu X. (2011) Microwave hydrothermal synthesis of $AgInS_2$ with visible light photocatalytic activity. *Mater. Res. Bull.,* 46, 975-982.
11. Friedmann D., Mendive C., Bahnemann D. (2010) TiO_2 for water treatment: Parameters affecting the kinetics and mechanisms of photocatalysis. *Appl. Catal. B: Environ.,* 99, 398-406.
12. Lei G., Xu M., Sun M., Fang H. (2006) Fabrication and characterization of nano TiO_2 thin films at low temperature. *Mater. Res. Bull.,* 41, 1596-1603.
13. Chen Y., Dionysiou D. D. (2006) Effect of calcination temperature on the photocatalytic activity and adhesion of TiO_2 films prepared by the P-25 powder-modified sol–gel method. *J. Mol. Catal. A: Chem.,* 244, 73-82.
14. Wada T., Kinoshita H., Kawata S. (2003) Preparation of chalcopyrite-type $CuInSe_2$ by non-heating process. *Thin Solid Film,* 431-432, 11-15.
15. Mao B., Chuang C. H., Wang J., Burda C. (2011) Synthesis and Photophysical Properties of Ternary I-III-VI $AgInS_2$ Nanocrystals: Intrinsic versus Surface States. *J. Phys. Chem. C.,* 115, 8945-8954.
16. Tian L., Vittal J. J. (2007) Synthesis and characterization of ternary $AgInS_2$ nanocrystals by dual- and multiple-source methods. *New J. Chem.,* 31, 2083-2087.
17. Yoshino K., Komaki H., Kakeno T., Akaki Y., Ikari T. (2003) Growth and characterization of p-type $AgInS_2$ crystals. *J. Phys. Chem. Solid,* 64, 1839-1842.
18. Lopez M. O., Galan O. V., Candarilla F. C. (2003) Preparation of $AgInS_2$ chalcopyrite thin films by chemical spray pyrolysis. *Mater. Res. Bull.,* 38, 55-61.
19. Aissa Z., Bouzidi A., Amlouk M. (2010) Study of the I–V characteristics of SnO_2:F/$AgInS_2$ (p)/Al Schottky diodes. *J. Alloys Compd.,* 506, 492-495.
20. Tadjarodi A., Cheshmekhavar, A. H., Imani, M. (2012) Preparation of $AgInS_2$ nanoparticles by a facile microwave heating technique; study of effective parameters, optical and photovoltaic characteristics. *Appl. Surf. Sci.,* 263, 449–456.
21. Ge S., Shui Z., Zheng Z., Zhang L. (2011) A general microwave-assisted nonaqueous approach to nanocrystalline ternary metal chalcogenide and the photoluminescence study of $CoIn_2S_4$. *Opt. Mater.,* 33, 1174-1178.
22. Zhang Y., Feng S. B., Wang K., Yi X. H., Wang H. S., Pan Y. M. (2012) Water-solvent method for the synthesis of N-substituted and N-,4-disubstituted 1,8-naphthalimides under microwave irradiation. *Synth. Commun.,* 42, 3042-3052.
23. Landry C. C., Lockwood J., Barron A. R. (1995) Synthesis of chalcopyrite semiconductors and their solid solutions by microwave irradiation. *Chem. Mater.,* 7, 699-706.
24. Cui Y., Ren J., Chen G., Qian Y., Xie Y. (2001) A simple route to synthesize $MInS_2$ (M= Cu, Ag) nanorods from single-molecule precursors. *Chem. Lett*., 236–237.
25. Gardner J. S., Shurdha E., Wang C., Lau L. D., Rodriguez R. G., Pak J. J. (2008) Rapid synthesis and size control of $CuInS_2$ semi-conductor nanoparticles using microwave irradiation, *J. Nanopart. Res.,* 10, 633–641.
26. Hu J. Q., Deng B., Tang K. B., Wang C. R., Qian Y. T. (2001) Preparation and phase control of nanocrystalline silver indium sulfides *via* a hydrothermal route, *J. Mater. Res.* 16, 3411–3415.
27. Nutek Inc. (2001) DOE-I basic design of experiments, *Quality Engineering Seminar and Software Version: 080617*, USA, Bloomfield Hills, MI.
28. Tadjarodi A., Imani M. (2011) Synthesis and characterization of CdO nanocrystalline structure by mechanochemical method, *Mater. Lett.* 65,1025–1027.